

See discussions, stats, and author profiles for this publication at: <https://www.researchgate.net/publication/276918268>

# One-Step Deposition of Photovoltaic Layers Using Iodide Terminated PbS Quantum Dots

ARTICLE *in* JOURNAL OF PHYSICAL CHEMISTRY LETTERS · NOVEMBER 2014

Impact Factor: 7.46 · DOI: 10.1021/jz502092x

---

CITATIONS

6

---

READS

45

## 9 AUTHORS, INCLUDING:



[Hyekyoung Choi](#)

Korea University of Science and Technology

15 PUBLICATIONS 84 CITATIONS

[SEE PROFILE](#)



[Hyungcheoul Shim](#)

Korea Institute of Machinery and Materials

21 PUBLICATIONS 191 CITATIONS

[SEE PROFILE](#)



[Matthew C Beard](#)

National Renewable Energy Laboratory

114 PUBLICATIONS 7,874 CITATIONS

[SEE PROFILE](#)



[Sohee Jeong](#)

Korea Institute of Machinery and Materials

62 PUBLICATIONS 848 CITATIONS

[SEE PROFILE](#)

## One-Step Deposition of Photovoltaic Layers Using Iodide Terminated PbS Quantum Dots

Sungwoo Kim,<sup>†,§</sup> Jaehong Noh,<sup>†</sup> Hyekyoung Choi,<sup>†,#</sup> Heonseok Ha,<sup>†</sup> Jung Hoon Song,<sup>†</sup> Hyung Cheoul Shim,<sup>†</sup> Jihoon Jang,<sup>†</sup> Matthew C. Beard,<sup>\*,†,§</sup> and Sohee Jeong<sup>\*,†,#</sup>

<sup>†</sup>Nanomechanical Systems Research Division, Korea Institute of Machinery and Materials, Daejeon 305-343, Republic of Korea

<sup>#</sup>Department of Nanomechatronics, University of Science and Technology, Daejeon 305-350, Republic of Korea

<sup>§</sup>National Renewable Energy Laboratory, Golden, Colorado 80401, United States

### Supporting Information

**ABSTRACT:** We present a one-step layer deposition procedure employing ammonium iodide ( $\text{NH}_4\text{I}$ ) to achieve photovoltaic quality PbS quantum dot (QD) layers. Ammonium iodide is used to replace the long alkyl organic native ligands binding to the QD surface resulting in iodide terminated QDs that are stabilized in polar solvents such as *N,N*-dimethylformamide without particle aggregation. We extensively characterized the iodide terminated PbS QD via UV-vis absorption, transmission electron microscopy (TEM), thermogravimetric analysis (TGA), FT-IR transmission spectroscopy, and X-ray photoelectron spectroscopy (XPS). Finally, we fabricated PbS QD photovoltaic cells that employ the iodide terminated PbS QDs. The resulting QD-PV devices achieved a best power conversion efficiency of 2.36% under ambient conditions that is limited by the layer thickness. The PV characteristics compare favorably to similar devices that were prepared using the standard layer-by-layer ethanethiol (EDT) treatment that had a similar layer thickness.

### SECTION: Physical Processes in Nanomaterials and Nanostructures



Recently, colloidal quantum dots (QDs) are being developed due to their beneficial optical properties such as band gap tunability, strong absorption over a broad wavelength region, an intrinsically large dipole moment, photostability, and enhanced multiple exciton generation (MEG).<sup>1–6</sup> In particular, the unique properties of QDs could greatly benefit solar energy conversion technologies because a QD-PV platform can be solution processed at low temperatures, yielding a flexible thin-film PV technology with reduced fabrication cost. Accordingly, studies have been undertaken to develop QD-PV approaches using QDs of inorganic metal chalcogenides such as  $\text{PbS}$ ,<sup>7,8</sup>  $\text{PbSe}$ ,<sup>9</sup>  $\text{HgTe}$ ,<sup>10</sup> and  $\text{CuIn}_{1-x}\text{Te}_{2-x}\text{Se}_x$ .<sup>11</sup>

The main factors that limit progress in further improving QD-PV are (1) developing an optimized PV architecture with appropriate contact layers and (2) improving QD-QD interfacial contact and surface passivation so as to achieve long charge-carrier diffusion lengths. The charge-carrier transport through the QD arrays and, therefore, PV performance depend on many factors, but the ligands play a major role. In general, as-prepared PbS QDs have long alkyl chain organic ligands, such as oleic acid (OA), which act as large insulating barriers to impede interparticle charge transfer. Therefore, the long alkyl surfactant is often replaced by a shorter molecule to reduce the distance between PbS QDs; common examples in the literature include, 1,2-ethanedithiol (EDT), 3-mercaptopropionic acid (MPA), and hydrazine.<sup>2,16,17</sup> Employing

conductive ligands is another approach and Talapin and co-workers have spearheaded the use of inorganic molecular metal chalcogenide surface ligands (MCCs) and chalcogenide ions such as  $\text{Sn}_2\text{S}_6^{4-}$ ,  $\text{In}_2\text{Se}_4^{2-}$ ,  $\text{S}^{2-}$ ,  $\text{Se}^{2-}$ ,  $\text{Te}^{2-}$ ,  $\text{HSe}^-$ , respectively.<sup>18–20</sup> Murray and co-workers reported a facile and versatile ligand exchange that modifies QD using a  $\text{NOBF}_4$  treatment.<sup>21</sup>

Recently, halide terminated QDs have received consideration partly because halide termination resulted in improved PV performance and QD-layer stability.<sup>13–15,23,24</sup> In a previous publication, we proposed that the stability of halide treated PbSe QDs could be attributed to a  $\text{PbX}_2(\text{Cl}, \text{Br}, \text{I})$  passivation layer that preferentially terminates the  $\{100\}$  facets.<sup>25</sup> Among other potential benefits, halide ligands can also serve the role of n-type doping<sup>26</sup> and they could remove detrimental midgap trap states.<sup>27</sup> Recent efforts have focused on constructing heterojunction PV architectures using halide treated QDs to achieve power conversion efficiencies (PCEs) of ~7%.<sup>22,23,28</sup> Further advances resulted in PCEs as high as 8.55% using a combination of halide and EDT treated QD layers.<sup>29</sup> However, in all these cases to obtain efficient device performance, a layer-by-layer (LBL) fabrication process is used to deposit the  $\text{PbS}(\text{Se})$  QDs. However, such a process is time-consuming

**Received:** October 1, 2014

**Accepted:** October 31, 2014

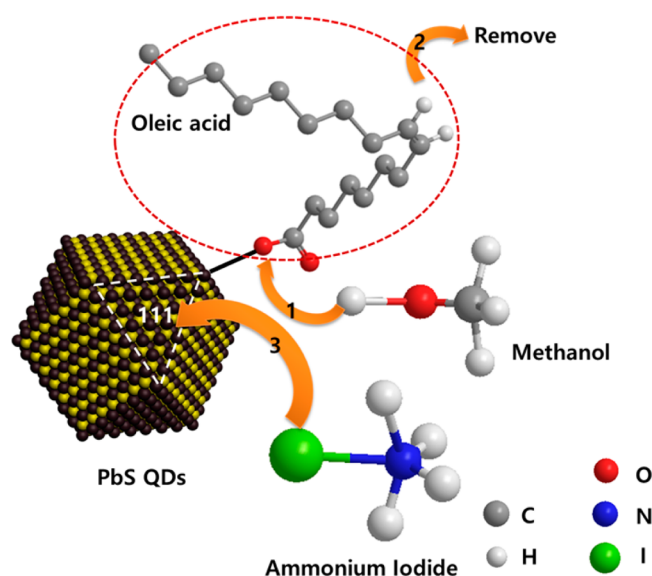
**Published:** October 31, 2014



because several tens of LBL cycles are needed in order to build-up a film of sufficient thickness. One reason for using a LBL process is because once the long alkyl-chain ligands have been removed from the QD they lose their colloidal stability, and thus, drop casting and spin-coating procedures are not suitable. As a result, attempts to fabricate QD layers by other means have been met with limited success. Sargent and co-workers reported the use of 1-thioglycerol (TG) terminated PbS QDs to perform a single layer drop casting process.<sup>30</sup> The work reported here focuses on improving the QD film density while maintaining stability. We developed a one-step layer deposition procedure using ammonium iodide as the QD ligand.

Our iodide ligand exchange methodology is depicted in Scheme 1, and specific details are provided in the Supporting

**Scheme 1. Schematic Illustration of the Iodide Ligand Exchange Methodology with Ammonium Iodide**



Information. When a high concentration of ammonium iodide ( $\text{NH}_4\text{I}$ ) in anhydrous methanol is added to a PbS QD dispersion in octane solution, the PbS QDs precipitate immediately upon shaking. In low concentrations, we found that the halide ion adds to the neutral  $\{100\}$  surfaces of the QD and protects them from oxidative attack.<sup>25</sup> In those studies, our data suggest that the OA ligands mainly bind to the polar  $\{111\}$  surfaces as X-type ligands and are not removed when low concentrations of ammonium halide are added. Here, we find that adding higher concentrations results in the complete removal of OA ligands and the subsequent loss of colloidal stability. Protic amines or short-chain alcohols can etch surface atoms terminated by X-type carboxylate ligands.<sup>31,32</sup> In our model, these X-type ligands (oleate) are preferentially bound to the  $\{111\}$  facet, and therefore, adding methanol results in exposed  $\{111\}$  surfaces that are then passivated by the iodide ions (Scheme 1). Because the  $\{100\}$  facets are terminated at lower concentrations, the resulting QDs are therefore completely terminated by the halide.<sup>25</sup> After the QDs have precipitated, the supernatant can be removed and the precipitated PbS QDs redispersed in a hydrophilic solvent, such as  $N,N$ -dimethylformamide (DMF). Figure 1a shows the absorption spectrum of the as-synthesized PbS QDs with OA ligands in tetrachloroethane (TCE) (red line) and iodide ligands in DMF (blue line). The inset of Figure 1a shows the

photographs of PbS QD solutions before (left) and after (right) iodide ligand exchange and demonstrates that prior to exchange the PbS QDs can not be dispersed into DMF, whereas after the exchange, the PbS QDs can not be dispersed into octane.

When we carried out the halide ligand exchange process, we found that  $\text{F}^-$  and  $\text{Cl}^-$  ligand-exchanged PbS QDs showed unfavorable redispersibility in DMF. According to the principle of hard and soft acids and bases (HSAB),  $\text{Pb}^{2+}$  is soft acid and the halides, which are Lewis bases bond in the order of  $\text{I}^- > \text{Br}^- > \text{Cl}^- > \text{F}^-$ . Thus, the strongest bond should be between  $\text{Pb}^{2+}$  and  $\text{I}^-$ . Thus, when the coordination is weak, PbS QDs are not stabilized leading to particle aggregation. Therefore, for the remainder of this study, we focus on iodide terminated QDs. In this study, the first excitonic peak of the OA terminated PbS QDs is located at 950 nm and is red-shifted by 10 nm upon iodide exchange. The red shift could be attributed to a change of the QD shape due to the relative selective bonding of iodide ion on the  $\{111\}$  compared with the  $\{100\}$  facets; alternatively, the shift could be attributed to an increase in electron or hole wave function delocalization due to the more polar environment. Other factors that could effect the red-shift or broadening are effective dielectric constant at the surface of QDs and radiative electronic coupling between QDs.<sup>34</sup>

Figure 1b shows the Fourier transform infrared (FT-IR) spectra of the PbS QDs before and after iodide ligands are exchanged. The OA-capped PbS QDs show strong vibration at 2924 and 2854  $\text{cm}^{-1}$  and at 1545 and 1403  $\text{cm}^{-1}$  that are associated with C–H and COO $^-$  vibration, respectively, which originate from the carboxylate groups in the OA ligands. However, significant reduction in the intensities of these peaks is observed in the iodide ligand exchanged sample, which indicates a complete substitution of OA with the iodide. Figure 1c shows the thermogravimetric analysis (TGA) data of PbS QDs before and after iodide ligand exchange, which measures the weight loss upon heating the sample from a low temperature to 400 °C under nitrogen. The weight loss of the iodide exchanged PbS (5.2%) is much lower than that of the OA terminated PbS QD samples (32%), providing further evidence for the complete ligand exchange from OA to iodide ligands.<sup>21</sup> The crystallinity of the particles was measured by X-ray diffraction (XRD) analysis before and after iodide ligand exchange, as shown in Figure 1d. The prominent peaks, which were indexed to the (111), (200), (220), (311), (222), (400), (331), (420), and (422) planes, indicate a rock salt structure corresponding to bulk PbS. The iodide ligand exchanged PbS QDs exhibited sharper (111) and (200) peaks than that of the OA-terminated PbS QDs. This may indicate that the iodide terminated PbS QDs have reconstructed surfaces and an altered shape due to the relative binding energies of iodide on the  $\{111\}$  and  $\{100\}$  surfaces.<sup>7,8</sup>

Such a conclusion is supported by Choi et al.,<sup>8</sup> who reported that oleate ligands bind preferentially on (111) facets and ligands can induce changes in NC shape based on both steric hindrance and selective ligand binding. Figure 2a and b show transmission electron microscopy (TEM) images of the synthesized PbS QDs before and after ligand exchange. The average diameter of the QDs is about 4.6 nm, consistent with the standard sizing curves<sup>12</sup> that relate the QD diameter to the first exciton transition energy. High resolution (HR) TEM images (Supporting Information Figure S1) also show that the average interparticle spacing is decreased from 3.5 nm with the OA ligands to 0.5 nm with iodide ligands, further confirming complete ligand exchange from OA to iodide ligands. To

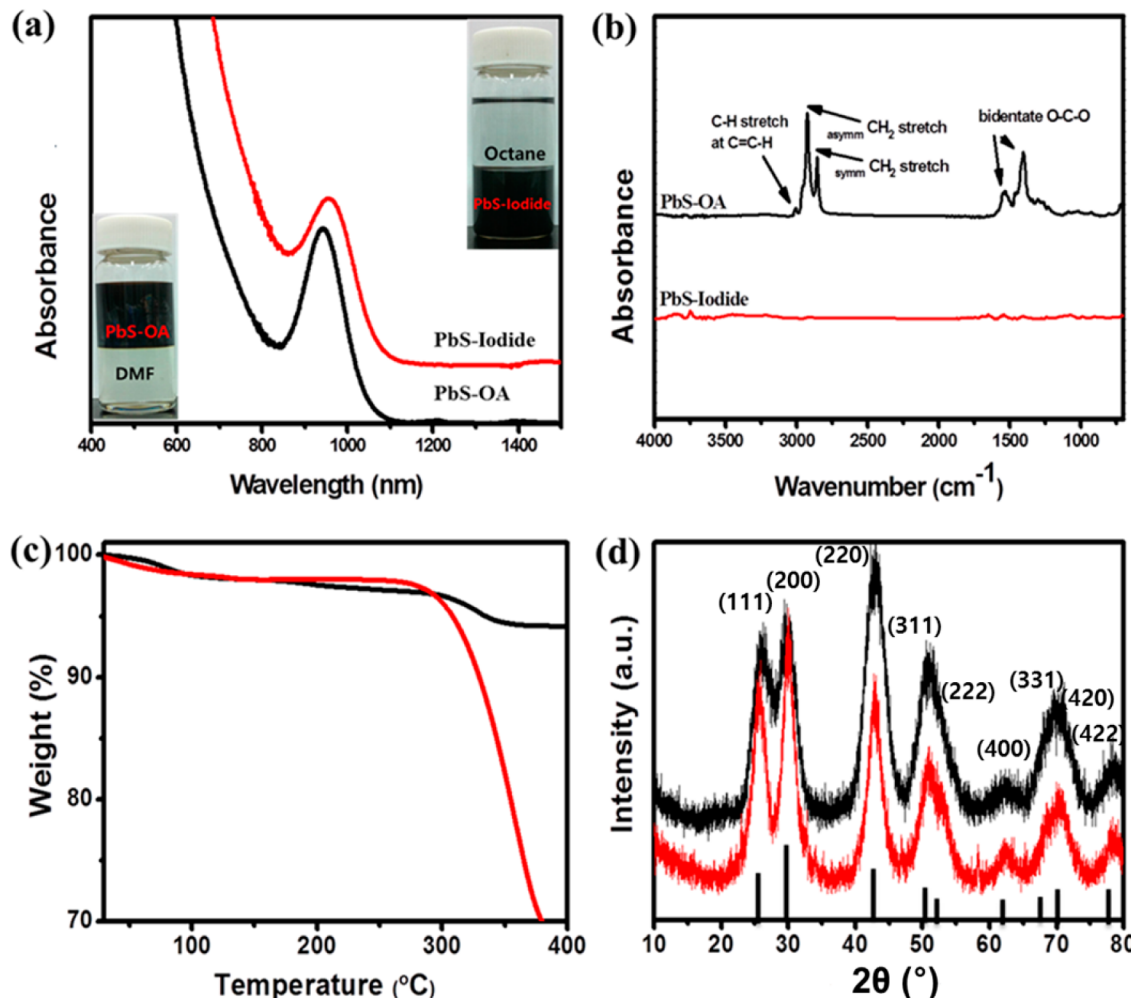


**Figure 1.** (a) UV–vis absorption spectrum of PbS QDs before (black) and after (red) iodide ligand exchange. (b) FT-IR spectra, (c) TGA, and (d) XRD data.

confirm the presence of iodide in the PbS QDs, we compare the X-ray photoelectron spectroscopy (XPS) results, shown in Figure 2c and d. From the Pb 4f high resolution XPS peak analysis, it is apparent that the iodide-terminated PbS QDs have binding energies that are higher, consistent with Pb–I bond formation (Pb–I bonding has a higher binding energy than Pb–S or Pb–O<sup>25</sup>), whereas the S 2s peak remained almost unchanged (Supporting Information Figure S2). There is a small peak at lower binding energy in the Pb 4f spectra of PbS-iodide QDs, which is not present for OA-PbS QDs. XPS peak deconvolution indicates that this arises from Pb–S bonding (Supporting Information Figure S3). Finally, I 3d<sub>5/2</sub> and 3d<sub>3/2</sub> peaks were observed at about 619.02 and 630.69 eV, respectively, which is similar to the binding of iodide atoms in the bulk state of PbI<sub>2</sub>.<sup>33</sup>

To determine whether the Pb–I termination can improve air stability, we stored the OA-PbS QD in TCE and I-PbS QDs in DMF in uncapped vials exposed to ambient conditions for 14 days. We then compared the absorption spectra and HR-XPS data for the OA and iodide terminated QDs (Supporting Information Figure S4). A blue shift is observed in the absorption spectrum of the OA-terminated QDs, whereas it does not shift for the iodide-terminated QDs, indicating that the PbS core is smaller in the OA-PbS samples, which is a common sign that indicates particle degradation. HR-XPS peak

analyses of the S 2p and Pb 4f, show that PbSO<sub>4</sub> or PbSO<sub>3</sub>, which are oxidation products, are prevalent for the OA terminated QDs, whereas the iodide terminated QDs only show slight degradation. We suppose that the improved stability of the iodide terminated QDs can be attributed to better protected {100} surfaces compared to oleate terminated QDs and the fact that iodide ions act as electron donors to prevent the oxidation.

We next developed a one-step deposition procedure to incorporate these iodide terminated QDs into a PV cell. The structure we tested is FTO/TiO<sub>2</sub>/PbS QD film/MoO<sub>x</sub>/Au/Ag (illustrated in Figure 3a). The PbS QDs were deposited on top of the TiO<sub>2</sub> via spin coating at 1000 rpm from a 200 mg/mL DMF solution. In order to promote adhesion of the PbS QDs to the TiO<sub>2</sub> surface, the TiO<sub>2</sub> layer was treated with a 20 wt % MPA linker in ethanol solution. The MPA acts as an anchor for PbS QDs onto the surface of TiO<sub>2</sub>. Using a cross-sectional TEM image (Figure 3b), the thickness of the photoactive layer was found to be ~150 nm. The EQE (or IQE) spectrum (Supporting Information Figure S10) shows that the device has a photoresponse to wavelengths up to ~1100 nm. Here, IQE is defined as EQE/(1 – R) where R is the light reflected from the solar cell device and, thus, does not account for light absorption within nonphotoactive regions of the device. Figure 3c and d are a magnified TEM image of the PbS QD-layer near the

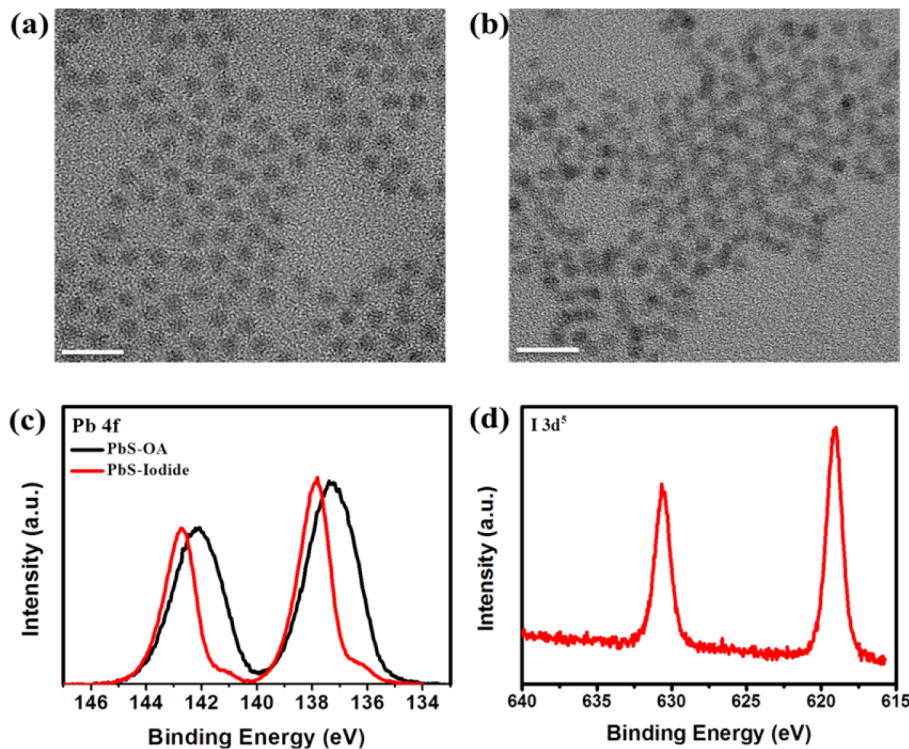


**Figure 2.** (a), (b) TEM images of PbS QDs before and after iodide ligand exchange, respectively. XPS spectrum of PbS QDs before and after iodide ligand exchange (scale bar = 10 nm) (c) Pb 4f spectrum. (d) I 3d spectrum of iodide ligand exchanged PbS QDs.

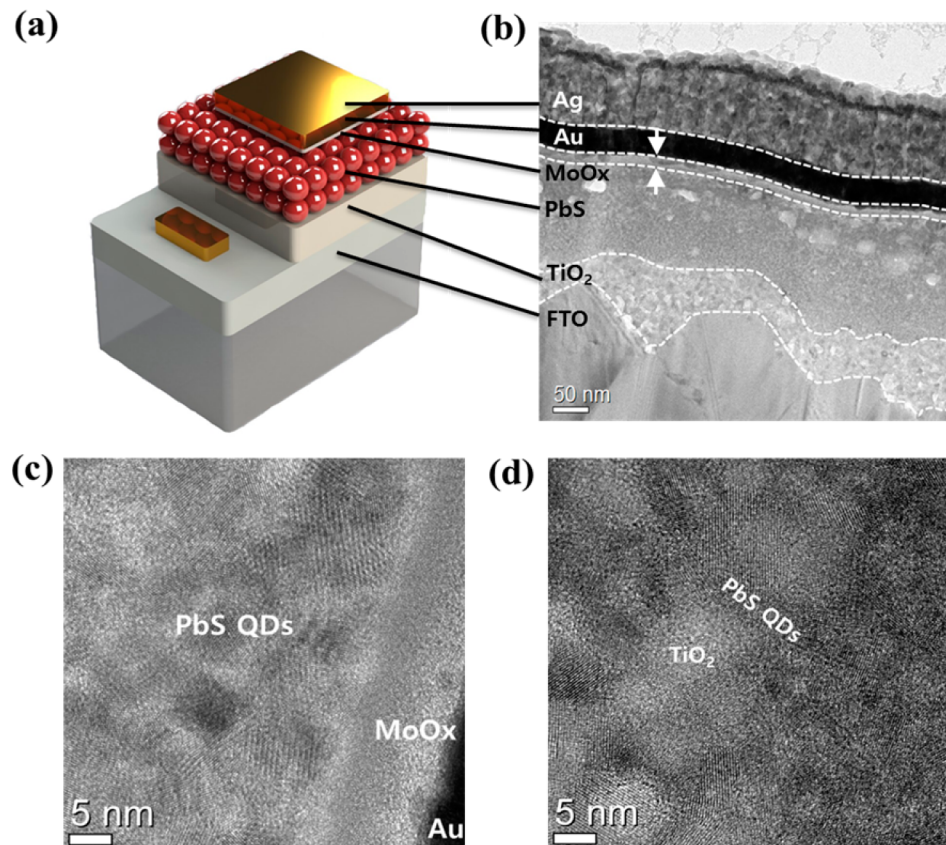


**Figure 3.** (a) Schematic illustration of the one-step deposited PbS CQD heterojunction device structure. (b) Cross-sectional TEM image of the as-made solar cell. (c) Cross-sectional HR-TEM image of PbS CQD photoactive layer near the PbS QD/MoO<sub>x</sub> interface and (d) the TiO<sub>2</sub>/ PbS QDs interface.

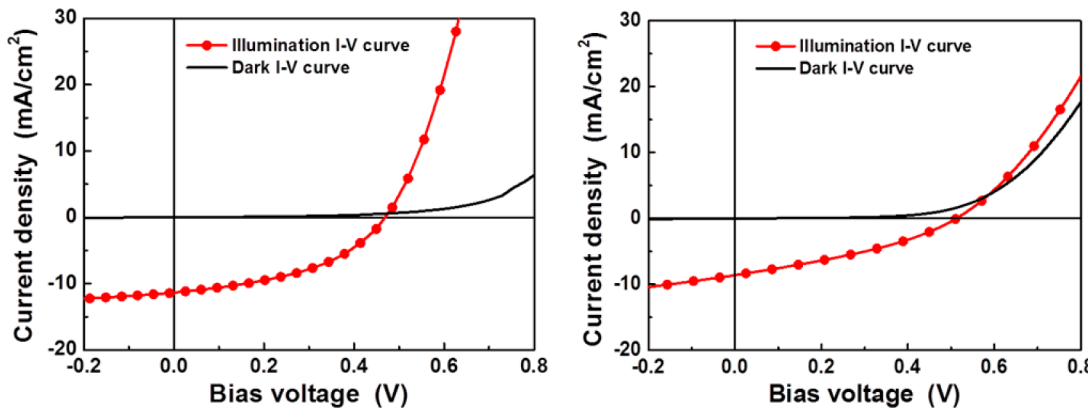


**Figure 4.**  $I$ - $V$  curves of the one-step deposited QDs film (left panel) and the LBL QDs film (right panel).

$\text{MoO}_3/\text{QD}$  and  $\text{TiO}_2/\text{QD}$  interface. Energy dispersive spectrometry (EDS) line profiles (Supporting Information Figure S5) indicate that the iodide terminated PbS QDs were deposited on the surface of the  $\text{TiO}_2$  layer. Also, STEM-EDS elemental mapping (Supporting Information Figure S6) shows that iodide (red) and lead (yellow-green) atom signals are uniformly distributed across the photoactive layer. To compare the device performance, we fabricated two devices with the same thickness of photoactive layers ( $\sim 150$  nm) and measured their  $J$ - $V$  curves at AM 1.5 illumination under ambient conditions. Standard deviation and histograms of the PV performance using iodide terminated PbS QDs are shown in Supporting Information Figure S8. Figure 4 shows the photocurrent density–voltage ( $J$ - $V$ ) curves of one-step deposited PbS QD and LBL PbS QD devices. The initial results of each best device performance are summarized in Table S1 (Supporting Information). The one-step deposition process ( $\sim 150$  nm) based PbS QD device showed a  $J_{\text{sc}}$  of  $11.38 \text{ mA cm}^{-2}$ ,  $V_{\text{oc}}$  of  $0.46 \text{ V}$ , FF 44.16%, and an overall power conversion efficiency ( $\eta$ ) of 2.36% under AM 1.5 illumination. The LBL process ( $\sim 150$  nm) based on EDT treated PbS QDs showed a  $J_{\text{sc}}$  of  $8.59 \text{ mA cm}^{-2}$ ,  $V_{\text{oc}}$  of  $0.50 \text{ V}$ , FF of 34.37%, and  $\eta$  of 1.504%. Thus, the improved device efficiency in the one-step deposition process based iodide terminated PbS QD device could be attributed to enhanced  $J_{\text{sc}}$ . From the  $J$ - $V$  characteristics, the devices developed here showed a series resistance ( $R_s$ ) of  $1.244 \Omega \text{ cm}^2$  and shunt resistance ( $R_{\text{sh}}$ ) of  $1.6821 \text{ k}\Omega \text{ cm}^2$ , whereas the LBL processed devices showed a  $R_s$  of  $77.488 \Omega \text{ cm}^2$  and  $R_{\text{sh}}$  of  $0.3006 \text{ k}\Omega \text{ cm}^2$ .

In summary, we presented a one-step deposition process employing ammonium iodide to fabricate heterojunction solar cells with efficiencies greater than 2% under ambient conditions. These strategies offer great potential to enable one-step deposited PbS QDs as an effective substitutes for LBL process for generating solution-processable, cost-effective energy conversion platforms. We are in the process of extending these concepts to thicker PbS QD layers, which should result in higher device efficiencies. Also, we are currently exploring spray coating for thicker layer formation with interface chemical modifications.

## ASSOCIATED CONTENT

### Supporting Information

Detailed experimental procedure, characterization, HR-TEM images, XPS S 2s, Pb 4f spectrum of PbS CQDs before and after iodide ligand exchange, EDS line profiles, mapping of

iodide capped PbS QDs film. Cross-sectional SEM images, standard deviation and histogram in the PV performance. EQE of the one-spin-deposited QDs and for the LBL QDs. Device performances are summarized Table S1. This material is available free of charge via the Internet at <http://pubs.acs.org>.

## AUTHOR INFORMATION

### Corresponding Authors

\*E-mail: sjeong@kimm.re.kr.

\*E-mail: matt.beard@nrel.gov.

### Notes

The authors declare no competing financial interest.

## ACKNOWLEDGMENTS

We acknowledge helpful comments and suggestions from Joseph M. Luther, Ryan Crisp, and Ashley Marshall. This work was supported by the Global Frontier R&D program by the Center for Multiscale Energy Systems (2011-0031566) and the Global R&D program (1415134409) funded by KIAT. M.C.B. acknowledges support from the Center for Advanced Solar Photophysics funded by the U.S. Department of Energy Office of Science, Office of Basic Energy Sciences Energy Frontier Research Centers program. DOE funding was provided to NREL through contract DE-AC36-08G028308.

## REFERENCES

- (1) Nozik, A. J.; Beard, M. C.; Luther, J. M.; Law, M.; Ellingson, R. J.; Johnson, J. C. Semiconductor Quantum Dots and Quantum Dot Arrays and Applications of Multiple Exciton Generation to Third-Generation Photovoltaic Solar Cells. *Chem. Rev.* **2010**, *110*, 6873.
- (2) Talapin, D. V.; Lee, J. S.; Kovalenko, M. V.; Shevchenko, E. V. Prospects of Colloidal Nanocrystals for Electronic and Optoelectronic Applications. *Chem. Rev.* **2010**, *110*, 389–458.
- (3) Schaller, R.; Klimov, V. High Efficiency Carrier Multiplication in PbSe Nanocrystals: Implications for Solar Energy Conversion. *Phys. Rev. Lett.* **2004**, *92*, 186601.
- (4) Semonln, O. E.; Luther, J. M.; Beard, M. C. Quantum Dots for Next-generation Photovoltaics. *Mater. Today* **2012**, *15*, 508–515.
- (5) Shabaev, A.; Efros, A. L.; Nozik, A. J. Multiexciton Generation by a Single Photon in Nanocrystals. *Nano Lett.* **2006**, *6*, 2856–2863.
- (6) Nozik, A. J. Multiple Exciton Generation in Semiconductor Quantum Dots. *Chem. Phys. Lett.* **2008**, *457*, 3–11.
- (7) Hines, M. A.; Scholes, G. D. Colloidal PbS Nanocrystals with Size-Tunable Near-Infrared Emission: Observation of Post-Synthesis Self-Narrowing of the Particle Size Distribution. *Adv. Mater.* **2003**, *15*, 1844–1849.

- (8) Choi, H.; Ko, J. H.; Kim, Y. H.; Jeong, S. Steric-Hindrance-Driven Shape Transition in PbS Quantum Dots: Understanding Size-Dependent Stability. *J. Am. Chem. Soc.* **2013**, *135*, 5278–5281.
- (9) Pietryga, J. M.; Schaller, R. D.; Werder, D.; Stewart, M. H.; Klimov, V. I.; Hollingsworth, J. A. Pushing the Band Gap Envelope: Mid-Infrared Emitting Colloidal PbSe Quantum Dots. *J. Am. Chem. Soc.* **2004**, *126*, 11752–11753.
- (10) Im, S. H.; Kim, H. J.; Kim, S. W.; Kim, S. W.; Seok, S. I. Efficient HgTe Colloidal Quantum Dot-Sensitized Near-Infrared Photovoltaic Cells. *Nanoscale* **2012**, *4*, 1581–1584.
- (11) Kim, S.; Kang, M.; Kim, S.; Heo, J.-H.; Noh, J. H.; Im, S. H.; Seok, S. I.; Kim, S.-W. Fabrication of CuInTe<sub>2</sub> and CuInTe<sub>2-x</sub>Se<sub>x</sub> Ternary Gradient Quantum Dots and Their Application to Solar Cells. *ACS Nano* **2013**, *7*, 4756–4763.
- (12) Moreels, I.; Lambert, K.; Smeets, D.; Muynck, D. D.; Nollet, T.; Martins, J. C.; Vanhaecke, F.; Vantomme, A.; Delerue, C.; Allan, G.; Hens, Z. Size-Dependent Optical Properties of Colloidal PbS Quantum Dots. *ACS Nano* **2009**, *3*, 3023–3030.
- (13) Tang, J.; Kemp, K. W.; Hoogland, S.; Jeong, K. S.; Liu, H.; Levina, L.; Furukawa, M.; Wang, X.; Debnath, R.; Cha, D.; et al. Colloidal Quantum Dot Photovoltaics Using Atomic-Ligand Passivation. *Nat. Mater.* **2011**, *10*, 765–771.
- (14) Ning, Z.; Voznyy, O.; Pan, J.; Hoogland, S.; Adinolfi, V.; Xu, J.; Li, M.; Kirmani, A. R.; Sun, J.-P.; Minor, J.; et al. Air-Stable N-Type Colloidal Quantum Dot Solids. *Nat. Mater.* **2014**, *13*, 822–828.
- (15) Ning, Z.; Ren, Y.; Hoogland, S.; Voznyy, Q.; Levina, L.; Stadler, P.; Lan, X.; Zhitomirsky, D.; Sargent, E. H. All-Inorganic Colloidal Quantum Dot Photovoltaics Employing Solution-Phase Halide Passivation. *Adv. Mater.* **2012**, *24*, 6295–6299.
- (16) Semonin, O. E.; Luther, J. M.; Choi, S.; Chen, H.-Y.; Gao, J.; Nozik, A. J.; Beard, M. C. Peak External Photocurrent Quantum Efficiency Exceeding 100% via MEG in a Quantum Dot Solar Cell. *Science* **2011**, *334*, 1530–1533.
- (17) Talapin, D. V.; Murray, C. B. PbSe Nanocrystal Solids for n- and p-Channel Thin Film Field-Effect Transistors. *Science* **2005**, *310*, 86–89.
- (18) Kovalenko, M. V.; Scheele, M.; Talapin, D. V. Colloidal Nanocrystals with Molecular Metal Chalcogenide Surface Ligands. *Science* **2009**, *324*, 1417–1420.
- (19) Kovalenko, M. V.; Bodnarchuk, M. I.; Zaumseil, J.; Lee, J.-S.; Talapin, D. V. Expanding the Chemical Versatility of Colloidal Nanocrystals Capped with Molecular Metal Chalcogenide Ligands. *J. Am. Chem. Soc.* **2010**, *132*, 10085–10092.
- (20) Nag, A.; Kovalenko, M. V.; Lee, J. S.; Liu, W. Y.; Spokoyny, B.; Talapin, D. V. Metal-Free Inorganic Ligands for Colloidal Nanocrystals: S<sub>2</sub><sup>-</sup>, HS<sup>-</sup>, Se<sup>2-</sup>, HSe<sup>-</sup>, Te<sup>2-</sup>, HTe<sup>-</sup>, TeS<sub>3</sub><sup>2-</sup>, OH<sup>-</sup>, and NH<sup>2-</sup> as Surface Ligands. *J. Am. Chem. Soc.* **2011**, *133*, 10612–10620.
- (21) Dong, A.; Ye, X.; Chen, J.; Kang, Y.; Gordon, T.; Kikkawa, J.; Murray, C. B. A Generalized Ligand-Exchange Strategy Enabling Sequential Surface Functionalization of Colloidal Nanocrystals. *J. Am. Chem. Soc.* **2011**, *133*, 998–1006.
- (22) Ip, A. H.; Thon, S. M.; Hoogland, S.; Voznyy, O.; Zhitomirsky, D.; Debnath, R.; Levina, L.; Rollny, L. R.; Carey, G. H.; Fischer, A.; et al. Hybrid Passivated Colloidal Quantum Dot Solids. *Nat. Nanotechnol.* **2012**, *7*, 577–582.
- (23) Zhang, J.; Gao, J.; Miller, E. M.; Luther, J. M.; Beard, M. C. Diffusion-Controlled Synthesis of PbS and PbSe Quantum Dots with in Situ Halide Passivation for Quantum Dot Solar Cells. *ACS Nano* **2014**, *8*, 614–622.
- (24) Zhang, J.; Gao, J.; Church, C. P.; Miller, E. M.; Luther, J. M.; Klimov, V. I.; Beard, M. C. PbSe Quantum Dot Solar Cells with More than 6% Efficiency Fabricated in Ambient Atmosphere. *Nano Lett.* **2014**, *14*, 6010–6015.
- (25) Woo, J. Y.; Ko, J.-H.; Song, J. H.; Kim, K.; Choi, H.; Kim, Y. H.; Lee, D. C.; Jeong, S. Ultrastable PbSe Nanocrystal Quantum Dots via in Situ Formation of Atomically Thin Halide Adlayers on PbSe(100). *J. Am. Chem. Soc.* **2014**, *136*, 8883–8886.
- (26) Zhitomirsky, D.; Furukawa, M.; Tang, J.; Stadler, P.; Hoogland, S.; Voznyy, O.; Liu, H.; Sargent, E. H. N-Type Colloidal-Quantum-Dot Solids for Photovoltaics. *Adv. Mater.* **2012**, *24*, 6181–6185.
- (27) Ning, Z.; Ren, Y.; Hoogland, S.; Voznyy, O.; Levina, L.; Stadler, P.; Lan, X.; Zhitomirsky, D.; Sargent, E. H. All-Inorganic Colloidal Quantum Dot Photovoltaics Employing Solution-Phase Halide Passivation. *Adv. Mater.* **2012**, *24*, 6295–6299.
- (28) Kim, J.; Voznyy, O.; Zhitomirsky, D.; Sargent, E. H. 25th Anniversary Article: Colloidal Quantum Dot Materials and Devices: A Quarter-Century of Advances. *Adv. Mater.* **2013**, *25*, 4986–5010.
- (29) Chuang, C.-H. M.; Brown, P. R.; Bulovic, V.; Bawendi, M. G. Improved Performance and Stability in Quantum Dot Solar Cells Through Band Alignment Engineering. *Nat. Mater.* **2014**, *13*, 796–801.
- (30) Fischer, A.; Rollny, L.; Pan, J.; Carey, G. H.; Thon, S. M.; Hoogland, S.; Voznyy, O.; Zhitomirsky, D.; Kim, J. Y.; Bakr, O. M.; Sargent, E. H. Directly Deposited Quantum Dot Solids Using a Colloidally Stable Nanoparticle Ink. *Adv. Mater.* **2013**, *25*, 5742–5749.
- (31) Hassinen, A.; Moreels, I.; Nolf, K. D.; Smet, P. F.; Martins, J. C.; Hens, Z. Short-Chain Alcohols Strip X-Type Ligands and Quench the Luminescence of PbSe and CdSe Quantum Dots, Acetonitrile Does Not. *J. Am. Chem. Soc.* **2012**, *134*, 20705–20712.
- (32) Anderson, N. C.; Hendricks, M. P.; Choi, J. J.; Owen, J. S. Ligand Exchange and the Stoichiometry of Metal Chalcogenide Nanocrystals: Spectroscopic Observation of Facile Metal-Carboxylate Displacement and Binding. *J. Am. Chem. Soc.* **2013**, *135*, 18536–18548.
- (33) Zheng, Zhi.; Liu, A.; Wang, S.; Wang, Y.; Li, Z.; Lau, W. M.; Zhang, L. In Situ Growth of Epitaxial Lead Iodide Films Composed of Hexagonal Single Crystals. *J. Mater. Chem.* **2005**, *15*, 4555–4559.
- (34) Luther, J. M.; Law, M.; Song, Q.; Perkins, C. L.; Beard, M. C.; Nozik, A. J. Structural, Optical, and Electrical Properties of Self-Assembled Films of PbSe Nanocrystals Treated with 1,2-Ethanedithiol. *ACS Nano* **2008**, *2*, 271–280.